Artificial Rod and Cone Photoreceptors with Human-Like Spectral Sensitivities

Byeongho Park, Heehong Yang, Tai Hwan Ha, Hyun Seo Park, Seung Ja Oh, Yong-Sang Ryu, Youngho Cho, Hyo-Suk Kim, Juyeong Oh, Dong Kyu Lee, et al.

DOI: 10.1002/adma.((please add manuscript number))
Article type: Communication

Artificial Rod and Cone Photoreceptors with Human-like Spectral Sensitivities

Byeongho Park[1,2,†], Heehong Yang[3,†], Tai Hwan Ha[4], Hyun Seo Park[1], Seung Ja Oh[1], Yong-Sang Ryu[1], Youngho Cho[1,5], Hyo-Suk Kim[1,6], Juyeong Oh[1,2], Dong Kyu Lee[1], Chulki Kim[1], Taikjin Lee[1], Minah Seo[1], Jaebin Choi[1], Young Min Jhon[1], Deok Ha Woo[1], Seok Lee[1], Seok Hwan Kim[7], Hyuk-Jae Lee[5], Seong Chan Jun[2], Hyun Seok Song[8,9,], Tai Hyun Park[3,*] and Jae Hun Kim[1,*]*

[1]Korean Institute of Science and Technology, Seoul, 02792, Republic of Korea

[2]Department of Mechanical engineering, Yonsei University, Seoul, 03722, Republic of Korea

[3]School of Chemical and Biological Engineering, Seoul National University, Seoul, 08826, Republic of Korea

[4]Hazards Monitoring Bionanotechnology Research center, Korea Research Institute of Bioscience and Biotechnology (KRIBB), Daejeon, 34134, Republic of Korea

[5]College of Science and Technology, Kookmin University, Seoul, 02707, Republic of Korea

[6]Department of Electronics and Communications Engineering, Kwang-woon University, Seoul, 01890, Republic of Korea

[7]Department of Ophthalmology, Seoul National University Boramae Hospital, Seoul, 07061, Republic of Korea

[8]Division of Bioconvergence Analysis, Korea Basic Science Institute (KBSI), Daejeon, 34133, Republic of Korea

[9]Center for Convergent Research of Emerging Virus Infection, Korea Research Institute of Chemical Technology, Daejeon, 34114, Republic of Korea

[*] Dr. Hyun Seok Song

Division of Bioconvergence Analysis,

Korea Basic Science Institute (KBSI),

Daejeon, 34133, Republic of Korea

Center for Convergent Research of Emerging Virus Infection,

Korea Research Institute of Chemical Technology,

Daejeon, 34114, Republic of Korea

E-mail: hssong7@kbsi.re.kr

Prof. Tai Hyun Park

School of Chemical and Biological Engineering,

Seoul National University,

Seoul, 08826, Republic of Korea

E-mail: thpark@snu.ac.kr

Dr. Jae Hun Kim

Sensor-system research center,

Korean Institute of Science and Technology,

Seoul, 02792, Republic of Korea

E-mail: jaekim@kist.re.kr

† These authors contributed equally to this work.

Keywords: color sensitivity, graphene, human-like artificial material, photoreceptor, spectral characteristic

Photo-sensitive material, which needs biologically engineered elements and delicate techniques with high efficiency, stability, and biocompatibility, has not yet been well-developed to replace damaged visual-systems to detect light and transfer signal into a neuron in our body. In current study, artificial nanovesicle based photo-sensitive materials were found to possess the characteristics of human-like photoreceptors for the first time. They exhibited considerably effective spectral characteristics according to each pigment. Four photoreceptors originated from human-eye with color-distinguishability were produced in HEK-293 cell and partially purified in the form of nanovesicle. Under various wavelengths of visible lights, electrochemical measurements with graphene working electrode playing an important role in lipid bilayer deposition and oxygen reduction process were performed to analyze the physiological behavior and kinetics of photoreceptors. Four nanovesicles with different photoreceptors rhodopsin (Rho), short-, medium-, and long-wave sensitive opsin 1 (1SW, 1MW, 1LW) showed remarkable color dependent characteristics, consistent with those of natural human retina. With four different light-emitting-diodes for functional verification, photoreceptors embedded in nanovesicles remarkably represented particular color sensitivity. This work demonstrates the potential to be used as photoreceptor-based artificial retina with human-like spectral feature for successful recovery from blindness, and to be applied to light-activated platforms in biological optoelectronic industries.

Spectral characteristics of photoreceptors, the rod, and cone cells in retina that are sensitive to light have been considered to be necessary to determine the absorption of photo-pigments. They are important for investigating optical and electrical interactions between neighboring receptors. These characteristics are also essential to understand spectral input to neural signal for color perception and the development of artificial retina. When retina in eyes interacts with photons, rhodopsin and photopsin in photoreceptors contribute to photoreceptor's output signal as photopigment through seven transmembrane G protein-coupled receptor (GPCR) and vitamin A as derivatives of retinal [1]. Each photopigment has specific color response

according to its structure. Rhodopsin is specifically contrast sensitive for blue-green color while three different photopsins can highly absorb red, green, and blue colors, respectively. Using calculation under density functional theory, photonic response [2] and wavelength dependent sensitivity [3] have been studied with various retinal isomers and their analogs.

Absorbance-based optical experiments have been performed to explore the spectral features of the photoreceptor. These studies have provided well-known reference results [4]. Bacteriorhodopsin based photo-activity has been investigated using scanning probe technique, spin-dependent electrochemical cyclic voltammetry, and chronoamperometric measurements [5]. Such measurements have been performed using biological specimens and tissues of living organisms. These previous methods have been focused on denaturation for cell membrane, competition of ion behavior in limited outer cellular space, electrical coupling among different receptors, and cell return current caused by high resistance of basement membrane [6].

The objective of this study was to demonstrate empirical results for the color responses of artificially grown human photoreceptors with an opto-electrochemical experiment using four types of nanovesicle-based photoreceptors including rhodopsin and photopsins. Photoreceptors were partially purified using cell-derived nanovesicle method for signal generation [7]. Biochemical conversion of photoreceptors was then electrochemically analyzed. Voltammetry techniques with three electrodes were utilized for the electrochemical analysis of photochemical retinal transformation in photoreceptors intercalated in a vesicle-based lipid bilayer deposited on a graphene probe as a working electrode. Graphene- and carbon- based electrodes have been employed as biosensors due to their high conductivity and binding affinity for biomaterials. Since nanovesicles stimulated by photonic response on a graphene electrode could generate reduction peak-potential shift (RPS) in linear sweep voltammetry (LSV), color-distinguishability of artificially grown photoreceptors on vesicles was explored in this study by simple droplet voltammetry measurement.

Spectral characteristics of nanovesicle based photoreceptors were measured using electrochemical reaction (**Figure 1**). With monochromatic incident lights ranging from 420 nm to 600 nm in an interval of 10 nm, LSV results were obtained from screen printed sensor using graphene working electrode. To monitor ion channel behavior in the lipid bilayer deposited onto graphene sheets, repeated light exposure and LSV measurement were applied to the screen printed sensor with samples.

HEK-293 cells were transfected with mammalian expression vector containing human photoreceptor genes [rhodopsin (Rho), short wave sensitive opsin 1 (1SW), medium wave sensitive opsin 1 (1MW), and long wave sensitive opsin 1 (1LW) related to rod cell, blue cone, green cone, and red cone, respectively] (**Figure S1a**). Human photoreceptors were successfully expressed in HEK-293 cells **(Figure S1b**). They were mainly localized in cell membranes (**Figure S1c**). For visual signal processing activity, photoreceptors were bound with 11-*cis*-retinal using retinal-containing DMEM media. To determine the activity of photoreceptor in HEK-293 cells after 11-*cis*-retinal binding, calcium ion-selective Fluo-4 AM dye was used in calcium assay (**Figure S2**). Fluorescence emission was only detected for 11-*cis*-retinal-bound photoreceptors. Binding between human photoreceptor and 11-*cis*-retinal plays a key role in photonic response as described in previous works [8]. To partially purify human photoreceptors, cells were transfected with human photoreceptor genes to produce photoreceptor nanovesicles containing receptors on the surface. To prepare photoreceptor-nanovesicles, optimized method described in previous studies [7a, 9] was used. Results of western blot analysis of photoreceptor-nanovesicles achieved in HEK-293 cells are shown in **Figure 2a**. Bands of four different photoreceptors were clearly observed with expected sizes. The morphology of nanovesicle was monitored by field-emission SEM as shown in **Figure 2b and 2c**. These sphere-shaped nanovesicles composed of lipids were settled down on the glass surface. Their average diameter was ~ 500 nm in nanoscale. As represented in SEM images of **Figure 2**, photoreceptor-nanovesicles were successfully constructed. A schematic

diagram for the photoreceptor response of photoreceptor-nanovesicle to incident light is described in **Figure 2d**. Upon light activation on the photoreceptor, 11-*cis*-retinal is converted to all-*trans*-retinal in molecular scale along with overall structural change of the photoreceptor to reach thermodynamically stable state.

Screen printed electrode coated with reduced graphene oxide (RGO) as a working electrode was used to probe the opto-electrochemical response of photoreceptor-samples. As shown in **Figure 3a**, the working electrode had a sharp sheet structure and clean surface of typical graphene. A mushy and soft layer was observed from vesicle-deposited surface on RGO-based working electrode (**Figure 3b**). These vesicles were added onto the RGO surface, building a single lipid bilayer. With wide view of SEM images and XPS spectral results shown in **Figure S3**, the deposition of the lipid bilayer onto RGO was verified specifically. For phosphate buffered saline (PBS, buffer solution)-dropped graphene electrode, small salt particles were aggregated on the graphene surface (**Figure S3b**). Vesicles were settled down on the RGO surface or formed a single lipid bilayer (**Figure S3c**). In XPS results (**Figure S3d**), bare working electrode had a few oxygen bindings as RGO while nanovesicle-deposited graphene electrode provided broad and complex XPS peaks with various binding features due to bonding among lipids, proteins, and graphene. **Figure 3c** describes LSV results and vesicle-deposition process. As the vesicles settle down by sweeping the voltage, they form a lipid bilayer covering the graphene surface, which results in decreasing the absolute amount of current in voltammetry. During LSV measurement, charges were induced by electric potential on RGO working electrode. With the assistance of charges and oxygen-based functional groups on graphene surface, vesicles could be attracted rapidly [9b, 10]. After vesicle-deposition on working electrode, vesicles were ruptured and transformed into a single lipid bilayer and the surface was covered with its thin film [11]. RPS from positive to negative in linear voltammetry with reduction peak was focused in this study since our samples showed irreversible process without oxidation peak during positive potential sweep (**Figure S4**).

From LSV results shown in **Figure 4a**, RPS approached toward smaller absolute peak-potential value in our platform using consecutive measurements, including 10 times of light exposures. RPS of most samples started from -0.5 V and finished at near -0.45 V. However, current values of reduction peak were stable at near 15.5 μA during the entire measurement. Rho and 1LW photoreceptors represented intriguing RPS under white incident light according to exposure time, of which curves were saturated gently (**Figure 4b**). However, linear RPS of photoreceptor-nanovesicles was observed without any incident light (dark state, **Figure 4c**). Linear RPS was also observed from PBS buffer solution, and nanovesicles without photoreceptors in the presence or absence of incident light (**Figure S5**). Taken together, these results demonstrated that RPS of each element (either PBS or photoreceptors) was successfully derived by using deconvolution (**Figure S6**). Overall results from **Figure 4b,c**, **Figure S5**, and **Figure S6** clearly showed that these artificially produced and partially purified photoreceptors successfully interacted with incident light and devoted to saturation in RPS. A trend of linear shift in reduction peak was also observed with ferricyanide ($[Fe(CN)_6]^{3-}$), a standard material. The shift was found to be originated from electrode surface modification (**Figure S7**).

The reduction peak in LSV was due to oxygen reduction with four electron processes expressed in the following equation:

$$O_2 + 2H_2O + 4e^- \rightarrow 4OH^- \qquad (1)$$

Graphene-based electrode was investigated for oxygen reduction reaction as a metal-free electro catalyst that provided several reduction potentials with various pathways for the production of peroxide [12]. Surface condition of graphene-based electrode was changed after every voltammetry measurement, leading to RPS. PBS buffer contributed considerably to the surface alteration of graphene-based electrode after O_2 reduction since oxygen functional groups on the edge of graphene sheet participated in all LSV results, including steady RPS.

Curves of photoreceptor-nanovesicles with incident light were surprisingly saturated as shown in **Figure 4b**. Activated channels in single lipid bilayer might have played an important role in the variation of RPS since the surface property of RGO electrode to interact with oxygen in solution could be controlled by incident light (**Figure 4d and 4e**). Many studies have reported that there are various ion channels in mammalian membrane for ion exchanges in and out of cells. They act as switches with receptor proteins such as taste receptors [13], olfactory receptors [14], and dopamine receptors[9c]. Stimulation of photoreceptors by incident light can arouse the flux of specific ions through the ion channel into nanovesicles as described in **Figure 4d**. The number of activated channels on the RGO electrode was gradually increased with channel activation by photoreceptors under incident light, resulting in a saturating trend of RPS with gradient variation. Additionally, high bonding affinity between reduced all-*trans*-retinals and graphene surface might have contributed to RPS, similar to results of previous studies showing that glassy carbon electrode could attribute to RPS due to chemical reaction of all-*trans*-retinal with hydrogen in water during voltammetry measurement (**Figure 4e**) [15]. Reduced all-*trans* retinals are easily attached onto graphene sheets with thin layers, leading to the surface modification of the electrode. Two dominant reaction activities mentioned above (channel activation and morphological change on the surface) might have generated RPS variation with the surface property change of graphene electrode. Such method can be used to explore photoreceptors' spectral characteristics specifically with facile experimental setup and to obtain amplified signal from biomaterials.

Responses of four different photoreceptors to various incident lights with various wavelengths are shown in **Figure 5**. Representative curves provided differences in saturation point, slope change, and degree of RPS according to the wavelength of incident light (**Figure 5a-d**). This can be used to understand the spectral characteristics of samples indirectly under three-dimensional diagrams. To consider our results thoroughly, these curves were subjected

to saturation behavior analysis (**Figure S8**) [16]. The relative sensitivity was calculated against the time when it reached at the half of RPS saturation point with inverse proportion for the reaction rate. Each curve in **Figure S9** was fitted and computed to obtain a value of relative sensitivity from the whole data represented in **Figure 5a-d**. Rho sample showed a large RPS peak near 485 nm. Likewise, 1SW, 1MW, and 1LW provided the greatest RPS peaks at 440, 530, 556 nm, respectively. Similar results have been reported in previous studies on photoreceptors [17]. While most curves were increased gradually as samples were exposed to incident light, the saturation ratio was different according to varying wavelength. Artificially grown human photoreceptors had different sensitivities to corresponding wavelengths, comparable to previous results obtained from live animal models [6b-e]. As shown in **Figure 5e**, four types of artificially grown photoreceptors exhibited outstanding relative sensitivities, consistent with the results of absorbance spectrum obtained from human eyes [17]. By using Gaussian fitting method [18], fitting graph for specific sensitivity under different wavelengths of incident light was achieved as shown in **Figure 5e**.

To further investigate artificial photoreceptors, color distinguishability of our samples was evaluated using the following four types of light emitting diodes (LEDs) at the colors of blue (465 nm), green (520 nm), yellow (575 nm), and red (640 nm). As shown in **Figure 5f-i**, each cone receptor had different sensitivity according to each LED's emission wavelength. With blue and red LEDs, specific samples such as 1SW and 1LW reacted intensely. Green and yellow LEDs stimulated two types of samples (1MW and 1LW) according to their spectral characteristics. Our artificial human photoreceptors produced from the *in vitro* system had highly different responses to various wavelengths, leading to human-like light sensing. These functional verification suggest that the artificial human photoreceptors can be practically used in challenging fields such as artificial retina camera and biological imaging system.

In conclusion, versatile photoreceptor-nanovesicles were developed in this study to explore spectral characteristics of artificially grown human photoreceptors with relatively simple

method to enable mass-scale production. Color dependent physiological responses of these artificial biomaterials holding photoreceptors were demonstrated here for the first time. For electrochemical investigation, graphene working electrode was used to settle down nanovesicles rapidly, leading to a stable lipid bilayer on the surface. Oxygen reduction of the working electrode was changed by ion channel activation on membrane layer with photoreceptors and attachment of reduced all-*trans*-retinal onto graphene surface. RPS results were influenced by the wavelength of incident light. The saturation curve of RPS was subjected to mathematical analysis to understand the complex reaction of our bio-sample. Four types of photoreceptor-nanovesicles (Rho, 1SW, 1MW, and 1LW) showed fine sensitivity according to the wavelength of incident light. Even in the experiment with LEDs, our artificially grown photoreceptors provided color distinguishability similar to human photoreceptor cells. The approach presented herein can be applied to study physiological, biophysical, and biochemical processes in photoreceptors. It has considerable potential to be used to develop artificial retina technology.

Experimental Section

Cloning and expression of photoreceptors in HEK-293 cell. Genes of photoreceptors in pCMV6-entry vector were purchased from OriGene (USA). These photoreceptor genes were cloned into pcDNA3 mammalian expression vectors (Invitrogen, USA). Their sequences were confirmed by DNA sequencing (GenoTech, Korea). pcDNA3/*Rho-EGFP* and pcDNA3/*1LW-DsRed* were also constructed and confirmed by DNA sequencing. Human embryonic kidney (HEK)-293 cells were cultured with Dulbecco's Modified Eagles Medium (DMEM) (HyClone, USA) supplemented with 100 U/mL penicillin, 100 μg/mL streptomycin (Gibco, USA), and 10 % Fetal Bovine Serum (FBS) (Gibco, USA) at 37 ℃ and 5 % CO_2. Transfection was performed using Lipofectamine 3000 reagent (Invitrogen, USA) according to the manufacturer’s protocol. Transfected cells were harvested with phosphate-buffed saline (PBS,

pH 7.4) and lysed by sonication using Sonics Vibracell (USA) with 2 s on/off for 2 min. Western blot analysis was performed using anti-FLAG rabbit antibody (Cell Signaling Technology, USA) as primary antibody, HRP-conjugated anti-rabbit antibody (Millipore, USA) as secondary antibody, and Luminata Forte western HRP substrate (Millipore, USA).

Formation of nanovesicles expressing photoreceptors on surface. Cells were harvested and resuspended in DMEM containing 10 μM of 11-*cis*-retinal and 10 μg/mL of cytochalasin B (Sigma, USA) followed by agitation at 300 rpm for 30 min. Nanovesicles were separated from cells by centrifugation at 1000×g for 10 min. The supernatant was centrifuged at 15000×g for 30 min to collect nanovesicles. After the supernatant was removed, nanovesicles were produced and stored at -80 ℃. They were thawed before use. All procedures were performed in the dark. The shape of nanovesicles was observed by field emission scanning electron microscopy (SEM). These nanovesicles were applied onto poly-D-lysine-coated slide glass, washed with PBS, and fixed with 4% paraformaldehyde at room temperature for 20 min. Fixed nanovesicles were incubated with 1 % OsO_4 solution for 10 min, dehydrated with increasing concentrations of ethanol, and lyophilized with a freeze-dryer. Lyophilized nanovesicles were coated with Pt (10 nm) by sputter and visualized by SEM. Additionally, nanovesicles on graphene electrode after smooth air-dry and Pt (10 nm) coating were used for SEM images to monitor the intrinsic surface of the sample. The surface of graphene working electrode was analyzed using X-ray photoemission spectroscopy (XPS) (VG Scientific Instruments, ESCALAB 220i-XL).

Opto-electrochemical voltammetry measurements with three electrodes. Linear sweep voltammetry (LSV) was investigated by screen printed electrodes (SPE) (110GPH, Dropsens). Graphene was used as working electrode. Carbon was used as counter electrode while silver was used as reference electrode. A small drop of solution samples was employed onto the SPE surface. Using voltammetry analytical equipment (SP1, ZIVE LAB), induced potential was swept from 1 to -1 V. The current was detected under incident light with various

wavelengths ranging from 420 to 640 nm obtained from a supercontinuum white light source (SuperK CompacK, NKT Photonics). The specific wavelengths with different bandwidths were generated using Flexible Wavelength Selector (FWS-B-M, Spectrolight Inc.). As a stabilization process, LSV measurement for the graphene sheet was repeated 5 times to minimize residue on electrodes and build-up of lipid bilayer from nanovesicles on graphene working electrodes. For spectral responsivity measurement of photoreceptors, LSV measurement was performed after incident light was applied to the sample for a duration of 10 seconds. The process mentioned above was repeated 10 times to observe the overall electrochemical reaction of each photoreceptor.

Supporting Information

Supporting Information is available from the Wiley Online Library or from the author.

Acknowledgements

This research was supported by the National Research Foundation funded by the Korean government (MSIT) (NRF-2018R1A2B3004498). This project has received funding from the European Research Council (ERC) under the European Union's Horizon 2020 research and innovation programme (grant agreement No 682286). This study was also supported by KIST Institutional Program (2E27270), Samsung Research Funding Center of Samsung Electronics under Project Number SRFC-IT1701-02, and Korea Basic Science Institute (D37410).

Received: ((will be filled in by the editorial staff))

Revised: ((will be filled in by the editorial staff))

Published online: ((will be filled in by the editorial staff))

References

[1] S. Filipek, D. C. Teller, K. Palczewski, R. Stenkamp, *Ann. Rev. Biophys. Biomol. Struct.* **2003**, 32, 375.

[2] a) I. V. Rostov, R. D. Amos, R. Kobayashi, G. Scalmani, M. J. Frisch, *J. Phys. Chem. B.* **2010**, 114, 5547; b) I. V. Rostov, R. Kobayashi, R. D. Amos, *Mo. Phys.* **2012**, 110, 2329.

[3] a) C. S. López, O. N. Faza, S. L. Estévez, A. R. de Lera, *J. Comput. Chem.* **2006**, 27, 116; b) K. Fujimoto, J.-y. Hasegawa, H. Nakatsuji, *B. Chem. Soc. Jpn.* **2009**, 82, 1140; c) K. Fujimoto, S. Hayashi, J.-y. Hasegawa, H. Nakatsuji, *J. Chem. Theory. Comput.* **2007**, 3, 605.

[4] a) W. E. Smollon Jr, B. R. Wooten, B. R. Hammond, *Exp. Eye. Res.* **2015**, 140, 10; b) T. Lamb, *Vis. Res.* **1995**, 35, 3083.

[5] a) O. Berthoumieu, A. V. Patil, W. Xi, L. Aslimovska, J. J. Davis, A. Watts, *Nano. Lett.* **2012**, 12, 899; b) H. Einati, D. Mishra, N. Friedman, M. Sheves, R. Naaman, *Nano. Lett.* **2015**, 15, 1052.

[6] a) A. W. Snyder, R. Menzel, S. B. Laughlin, *J. Comp. Physiol. A* **1973**, 87, 99; b) K. Hamdorf, R. Paulsen, J. Schwemer, in *Biochemistry and physiology of visual pigments*, Springer **1973**, p. 155; c) S. Shaw, *Vis. Res.* **1969**, 9, 999; d) K. Kirschfeld, N. Franceschini, B. Minke, *Nature* **1977**, 269, 386; e) L. I. Brueggemann, J. M. Sullivan, *Biochemistry (Mosc.)* **2001**, 40, 4446.

[7] a) H. J. Jin, S. H. Lee, T. H. Kim, J. Park, H. S. Song, T. H. Park, S. Hong, *Biosens. Bioelectron.* **2012**, 35, 335; b) J. Park, J. H. Lim, H. J. Jin, S. Namgung, S. H. Lee, T. H. Park, S. Hong, *Analyst* **2012**, 137, 3249.

[8] a) S. Srinivasan, E. Ramon, A. Cordomí, P. Garriga, *Chem. Biol.* **2014**, 21, 369; b) M. R. Whorton, B. Jastrzebska, P. S.-H. Park, D. Fotiadis, A. Engel, K. Palczewski, R. K.

Sunahara, *J. Biol. Chem.* **2008**, 283, 4387; c) D. L. Farrens, H. G. Khorana, *J. Biol. Chem.* **1995**, 270, 5073.

[9] a) S. R. Ahn, J. H. An, H. S. Song, J. W. Park, S. H. Lee, J. H. Kim, J. Jang, T. H. Park, *ACS Nano* **2016**, 10, 7287; b) Y. Okamoto, K. Tsuzuki, S. Iwasa, R. Ishikawa, A. Sandhu, R. Tero, presented at *Journal of Physics: Conference Series* **2012**; c) S. J. Park, H. S. Song, O. S. Kwon, J. H. Chung, S. H. Lee, J. H. An, S. R. Ahn, J. E. Lee, H. Yoon, T. H. Park, *Sci. Rep.* **2014**, 4.

[10] R. Frost, G. E. Jönsson, D. Chakarov, S. Svedhem, B. Kasemo, *Nano. Lett.* **2012**, 12, 3356.

[11] a) R. Tero, *Materials* **2012**, 5, 2658; b) S. R. Tabaei, W. B. Ng, S.-J. Cho, N.-J. Cho, *ACS Appl. Mater. Interfaces.* **2016**, 8, 11875.

[12] a) J. Benson, Q. Xu, P. Wang, Y. Shen, L. Sun, T. Wang, M. Li, P. Papakonstantinou, *ACS Appl. Mater. Interfaces.* **2014**, 6, 19726; b) C. H. Choi, H.-K. Lim, M. W. Chung, J. C. Park, H. Shin, H. Kim, S. I. Woo, *J. Amer. Chem. Soc.* **2014**, 136, 9070; c) X. Ji, C. E. Banks, A. Crossley, R. G. Compton, *Chem. Phys. Chem.* **2006**, 7, 1337.

[13] H. S. Song, O. S. Kwon, S. H. Lee, S. J. Park, U.-K. Kim, J. Jang, T. H. Park, *Nano. Lett.* **2012**, 13, 172.

[14] T. H. Kim, S. H. Lee, J. Lee, H. S. Song, E. H. Oh, T. H. Park, S. Hong, *Adv. Mater.* **2009**, 21, 91.

[15] a) S. A. Wring, J. P. Hart, D. W. Knight, *Analyst* **1988**, 113, 1785; b) S. M. Park, *J. Electrochem. Soc.* **1978**, 125, 216.

[16] G. R. Kepner, *Theor. Biol. Med. Model.* **2010**, 7, 11.

[17] a) G. WALD, *Science* **1945**, 101, 653; b) P. K. Brown, G. Wald, *Science* **1964**, 144, 45.

[18] J. Carroll, M. Neitz, H. Hofer, J. Neitz, D. R. Williams, *Proc. Natl. Acad. Sci.*, **2004**, 101, 8461.

Figures

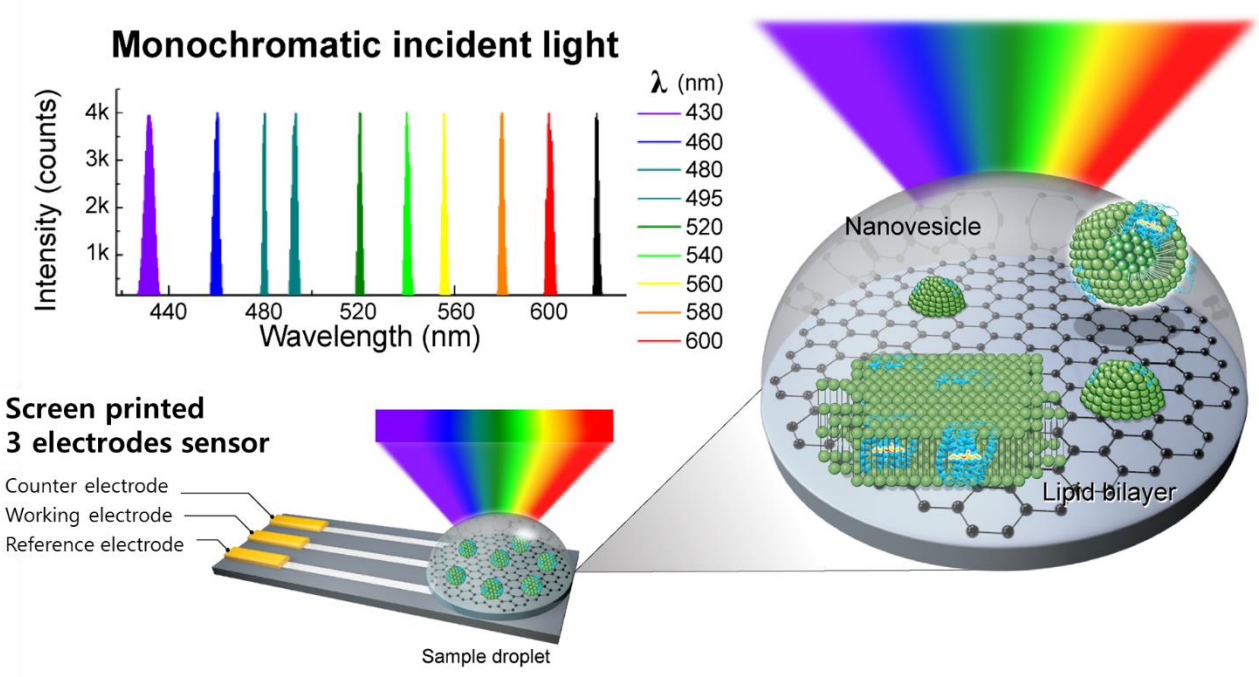

Figure 1. Schematic and opto-electrochemical experimental setup of three-electrode system for LSV with a single lipid bilayer deposited on graphene electrode of photoreceptor-nanovesicles.

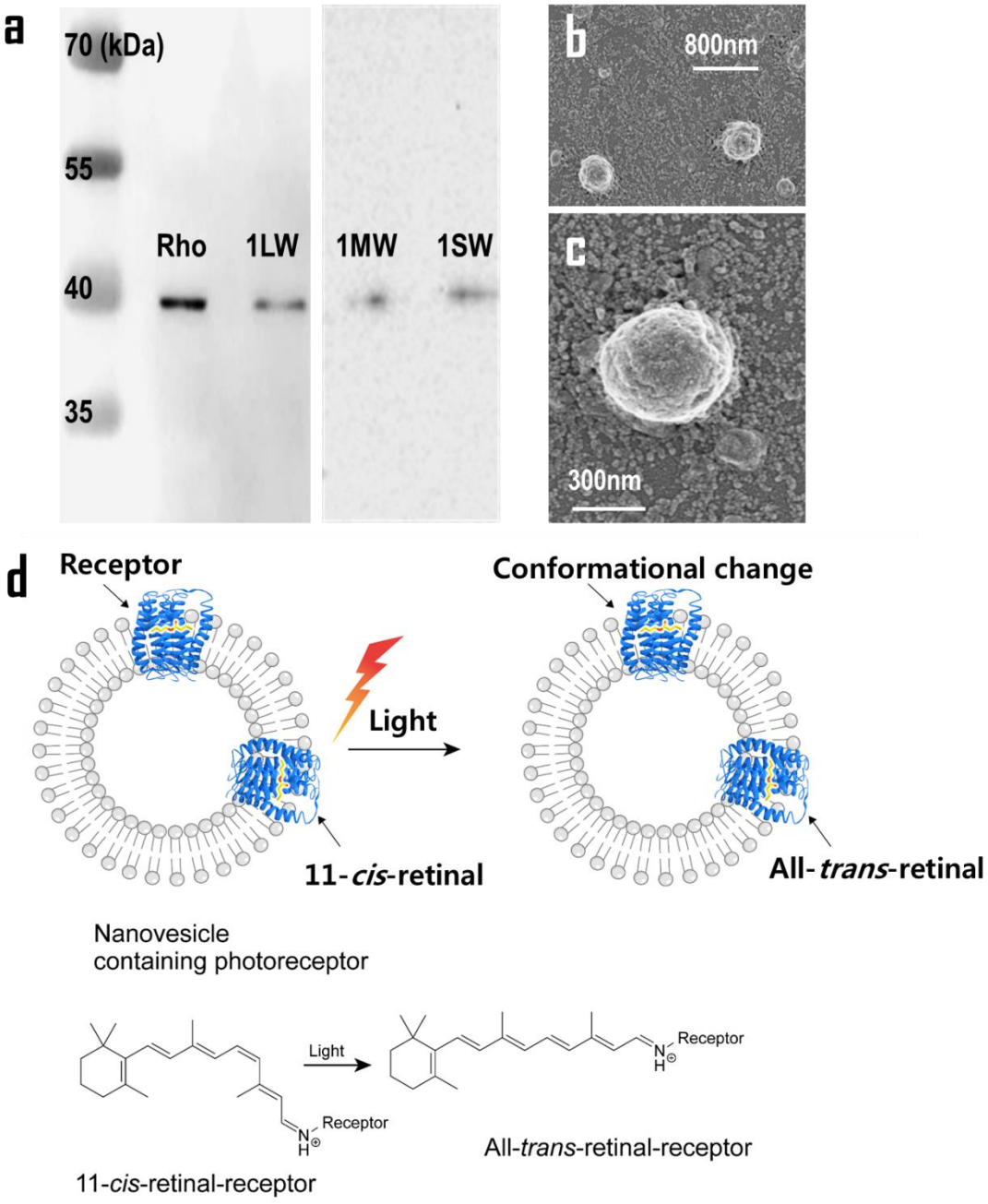

Figure 2. Preparation and characterization of human photoreceptors with 11-*cis* retinal. (a) Western blot analysis of photoreceptors expressed in HEK-293 cell using anti-FLAG antibody. Four types of photoreceptors were produced in nanovesicles. (b) SEM images of nanovesicles expressing photoreceptors on glass substrate surface. (c) Scale up view of specific nanovesicles. (d) Schematic of photo-induced reaction in nanovesicles containing photoreceptor with transformable retinal molecule under incident light.

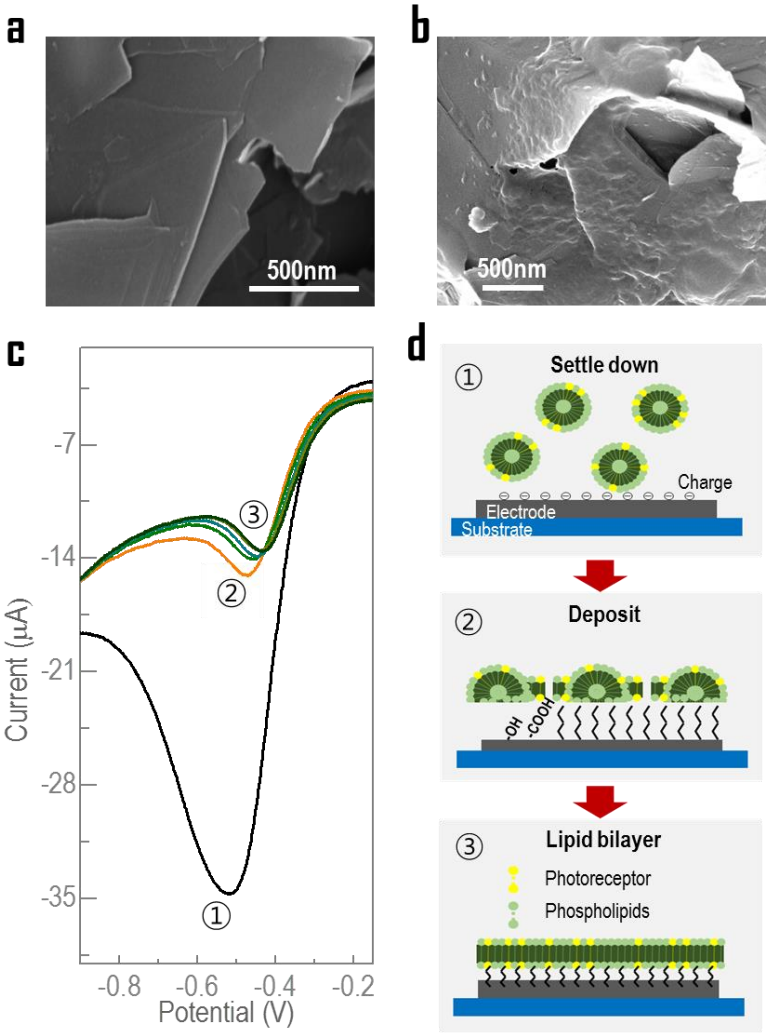

Figure 3. SEM images of graphene electrodes (a) before and (b) after vesicle deposit. (c) Linear sweep voltammetry results with samples including vesicles. (d) Schematics for vesicle deposition.

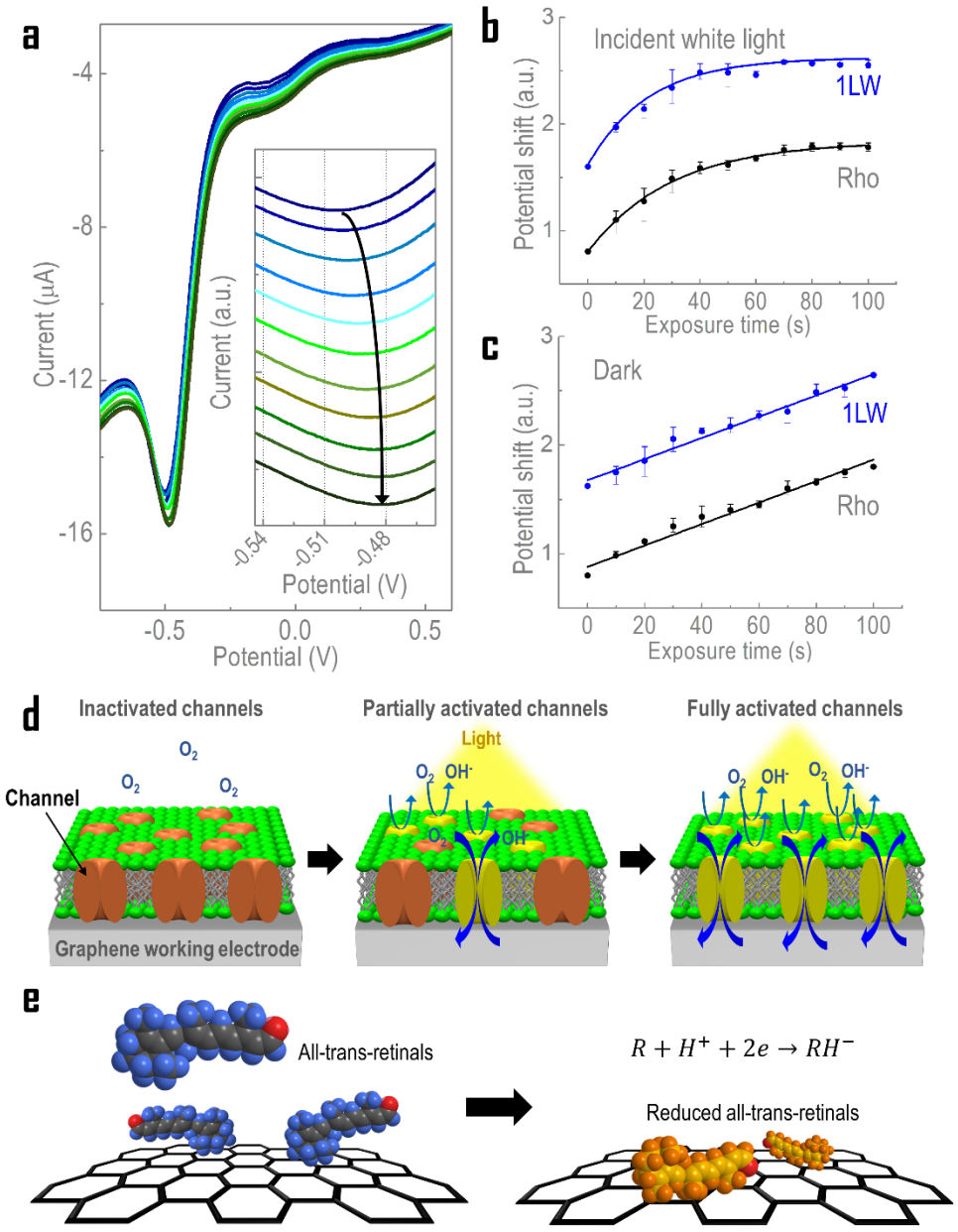

Figure 4. (a) Overall linear sweep potential result on graphene based and screen printed electrode according to elapsed light exposure time from 0 to 100 s. RPSs of Rho and 1LW samples from LSV with (b) incident white light and (c) in the dark. (d) Scheme of light-gated channel activation process by incident light and reduction of oxygen to hydroxide ion. (e) Scheme of attachment of electrochemical reaction products by all-*trans*-retinal on graphene surface.

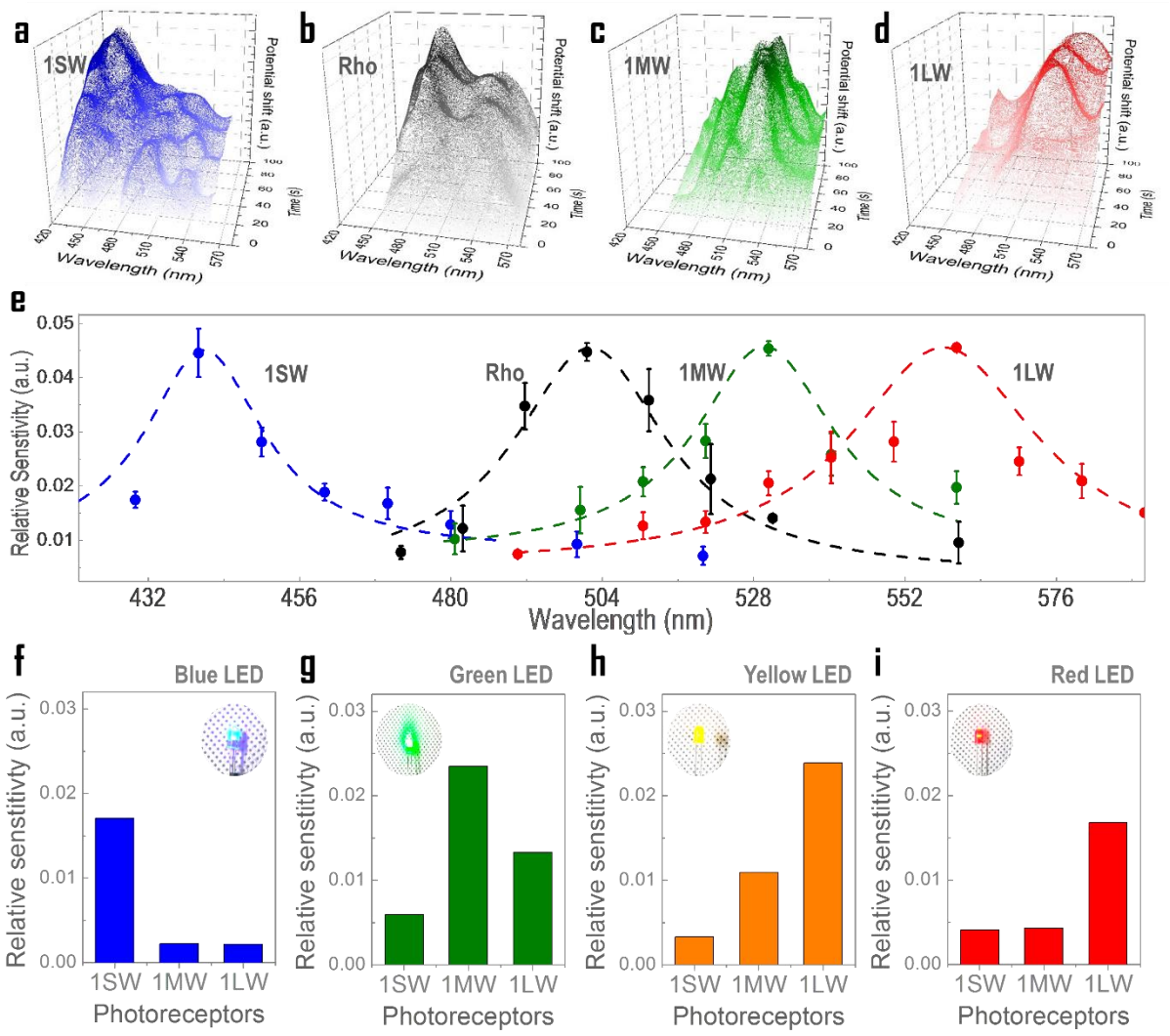

Figure 5. RPS results of (a) 1SW, (b) Rho, (c) 1MW, and (d) 1LW as a function of measuring time and wavelength of incident lights in visible wavelength ranging from 420 to 580 nm. (e) Relative sensitivity spectrum of all photoreceptor samples calculated using saturation behavior analysis. As functional verification, sensitivity comparison among samples using LED light sources with different emission: (f) blue, (g) green, (h) yellow, and (i) red.

Table of Contents

Artificially synthesized biological nanomaterials with four types of photoreceptors in nanovesicle show outstanding human-like spectral characteristics for visible light on a graphene working electrode for electrochemical measurement.

Keywords: color sensitivity, graphene, human-like artificial material, photoreceptor, spectral characteristic

Byeongho Park[1,2,†], Heehong Yang[3,†], Tai Hwan Ha[4], Hyun Seo Park[1], Seung Ja Oh[1], Yong-Sang Ryu[1], Youngho Cho[1,5], Hyo-Suk Kim[1,6], Juyeong Oh[1,2], Dong Kyu Lee[1], Chulki Kim[1], Taikjin Lee[1], Minah Seo[1], Jaebin Choi[1], Young Min Jhon[1], Deok Ha Woo[1], Seok Lee[1], Seok Hwan Kim[7], Hyuk-Jae Lee[5], Seong Chan Jun[2], Hyun Seok Song[8,9,], Tai Hyun Park[3,*] and Jae Hun Kim[1,*]*

Human-like Spectral Sensitivities of Artificial Rod and Cone Photoreceptors

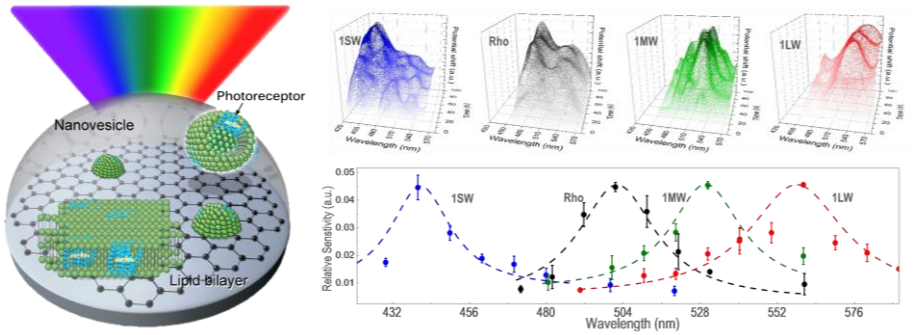

Supporting Information

Human-like Spectral Sensitivities of Artificial Rod and Cone Photoreceptors

Byeongho Park[1,2,†], Heehong Yang[3,†], Tai Hwan Ha[4], Hyun Seo Park[1], Seung Ja Oh[1], Yong-Sang Ryu[1], Youngho Cho[1,5], Hyo-Suk Kim[1,6], Juyeong Oh[1,2], Dong Kyu Lee[1], Chulki Kim[1], Taikjin Lee[1], Minah Seo[1], Jaebin Choi[1], Young Min Jhon[1], Deok Ha Woo[1], Seok Lee[1], Seok Hwan Kim[7], Hyuk-Jae Lee[5], Seong Chan Jun[2], Hyun Seok Song[8,9,], Tai Hyun Park[3,*] and Jae Hun Kim[1,*]*

Supplementary Methods

Confocal laser scanning microscopy (CLSM). Plasmids pcDNA3/*Rho-EGFP* and pcDNA3/*1LW-DsRed* were transfected into HEK-293 cells, respectively. Cells were fixed with 4% paraformaldehyde for 10 min at 37 ℃ and incubated with PBS (0.25% Trition X-100) for 10 min. Cells were also treated with DAPI (Thermo Fisher Scientific, USA) and washed with PBS. Fluorescences were detected using confocal microscopy (Olympus, USA).

Calcium flux assay of photoreceptors in HEK-293 cell. Transfected cells were incubated with 5 μM of fluo-4 AM (Molecular Probes, USA), 2.5 mM probenecid, and 10 μM of 11-*cis*-retinal (Santa Cruz Biotechnology, USA) in Ringer's solution (140 mM NaCl, 1 mM $MgCl_2$, 1.8 mM $CaCl_2$, 5 mM KCl, 5 mM glucose, 10 mM HEPES (pH 7.4)) at 37 ℃ for 1 hr. After three times of washing with Ringer's solution and further incubation for 30 min to remove nonspecific binding and allow complete de-esterification of AM esters, cells were imaged with a fluorescence microscope. All experiments were performed in the dark.

Supplementary Figures

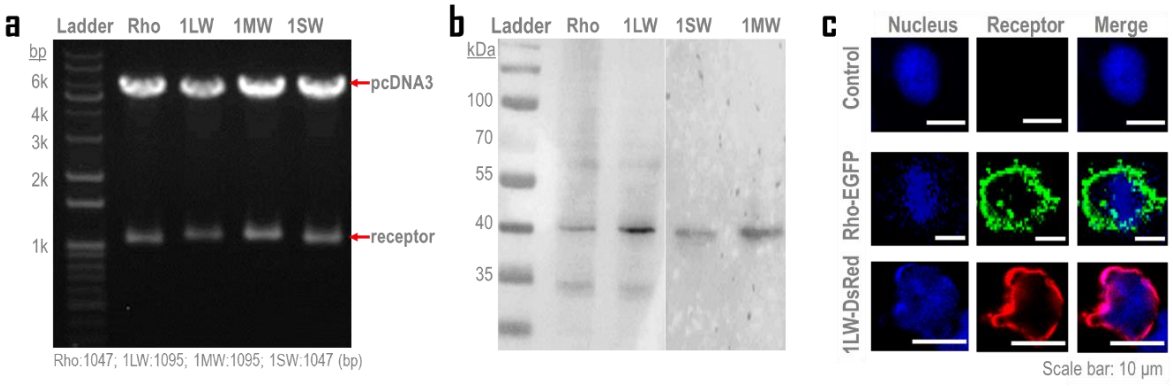

Figure S1. Cloning and expression of human photoreceptors. (a) Agarose gel electrophoresis of human photoreceptors. pcDNA3 expression vectors containing target genes were digested with *Eco*RI and XhoI. Genes of human photoreceptors [rhodopsin (Rho), short wave sensitive opsin 1 (1SW), medium wave sensitive opsin 1 (1MW), and long wave sensitive opsin 1 (1LW) related to rod cell, blue cone, green cone, and red cone, respectively] were cloned. (b) Western blot analyses of HEK-293 cells expressing photoreceptors. (c) Confocal laser scanning microscope (CLSM) images of HEK-293 cells expressing photoreceptors on membrane surface.

For mammalian expression of receptors, these photoreceptor genes were cloned into pcDNA3 mammalian expression vector and verified with agarose gel electrophoresis (**Fig. S1a**). The band of target DNA was confirmed by restriction enzyme digestion (*Eco*RI/*Xho*I) and the size of target gene was observed based on its expected size. Results showed that these pcDNA3 expression vectors containing genes of photoreceptors were successfully prepared. These photoreceptors were also successfully expressed in HEK-293 cells based on Western blot analysis (**Fig. S1b**). Bands of around 39 kDa were consistent with the expected sizes of these photoreceptors. Expressions of these photoreceptors on membrane surface were also monitored through CLSM images. **Fig. S1c** shows that fluorescences of the Rho-GFP and 1LW-DsRed are detected on the cell membrane. However, they were not observed control cells. These images demonstrated that cells transfected with Rho and 1LW expressed these

receptors on the membrane surface. These results indicated that human photoreceptors were successfully expressed in HEK-293 cell and these receptors were localized on the cell-surface of membrane.

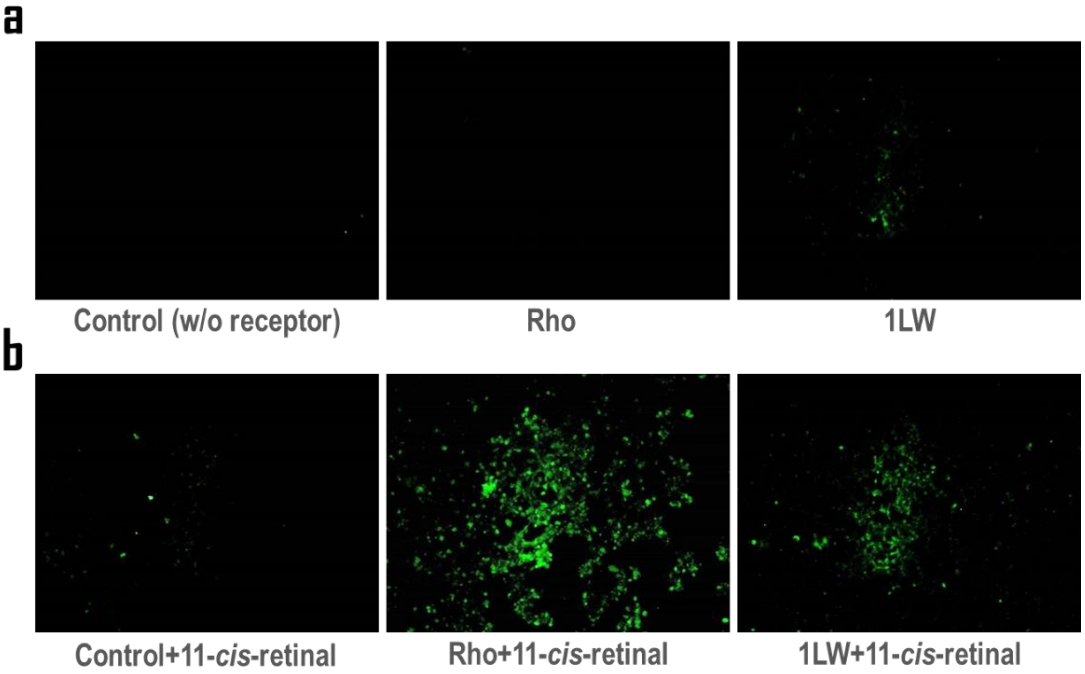

Figure S2. Calcium flux assays of HEK-293 cells expressing photoreceptors using Fluo-4 AM. Representative samples Rho nd 1LW were used for channel activating test. (a) In the presence of 11-*cis*-retinal. (b) In the absence of 11-*cis*-retinal. Fluorescence appeared only when 11-*cis*-retinal bound to photoreceptors.

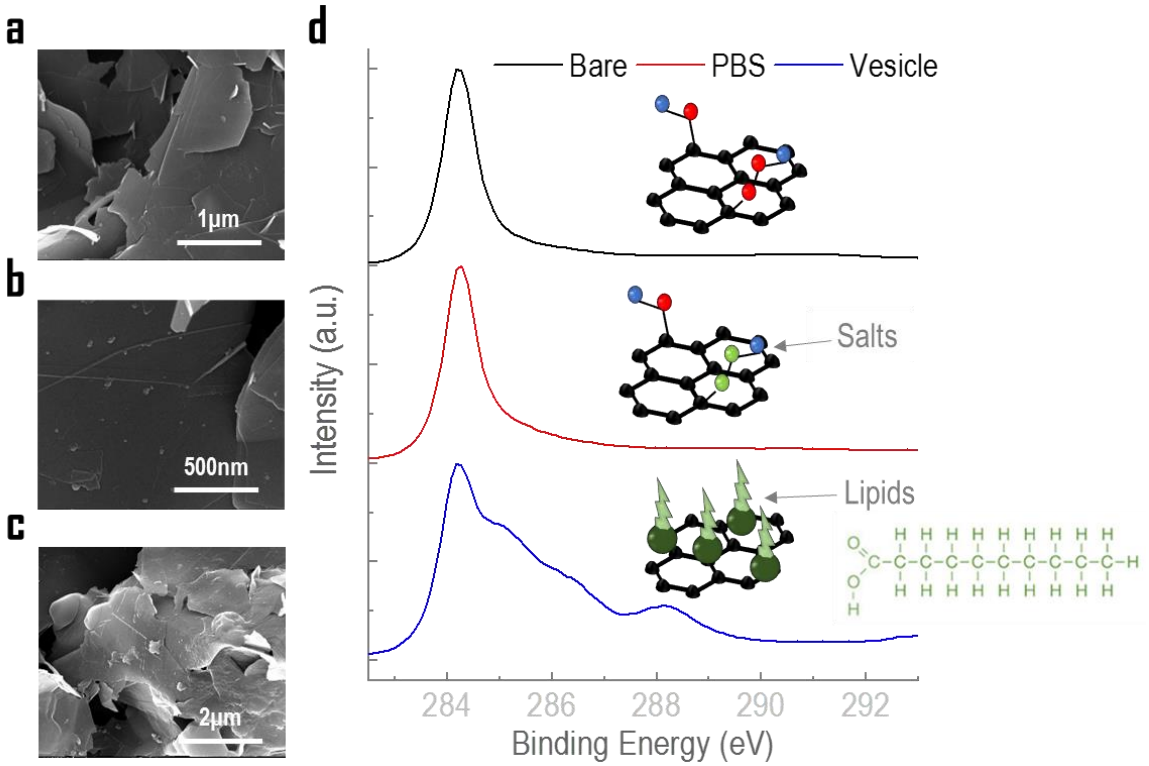

Figure S3. SEM images. (a) Bare working electrode surface, (b) PBS dropped and dried graphene. (c) Vesicle-deposited graphene electrodes. (d) XPS results of graphene electrode surface with bare working electrode, PBS-deposited electrode, and nanovesicle-deposited electrodes. Bare and PBS-deposited electrode has strong C-C bonding feature at 285 eV in the XPS result. Nanovesicle-deposited electrode has various bonding features from 285 to 289 eV within several bindings among lipids, proteins, and graphene.

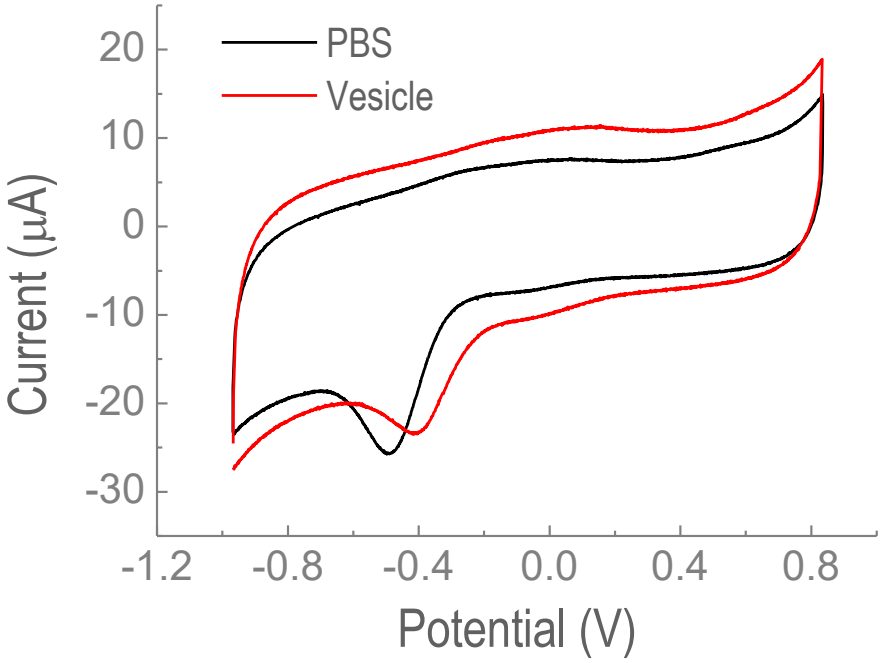

Figure S4. Cyclic voltammetry results of PBS buffer and vesicle sample.

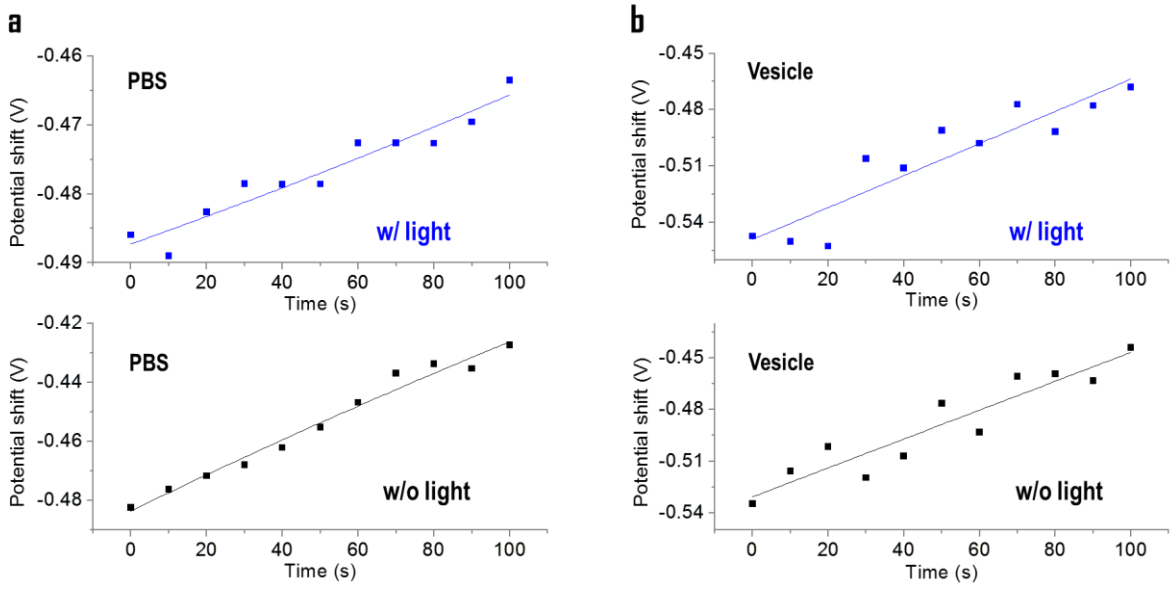

Figure S5. RPS of (a) PBS and (b) vesicle without photoreceptor in the presence or absence of incident light.

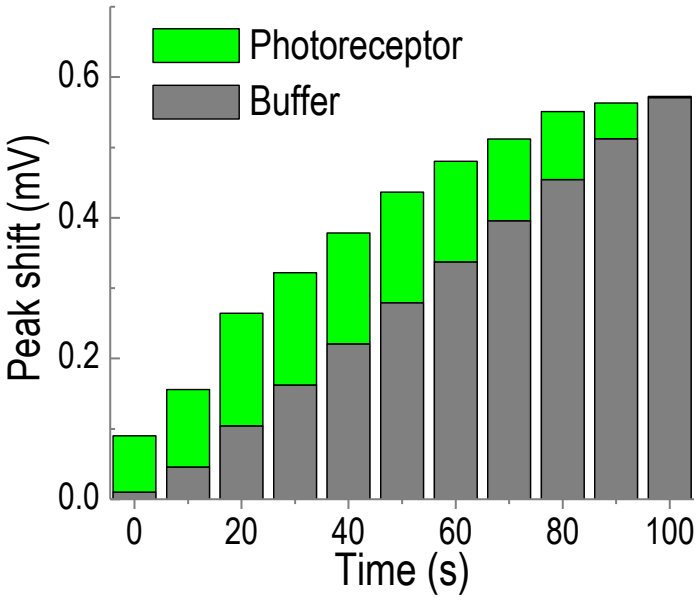

Figure S6. Bar diagram of RPS for photoreceptor-nanovesicles with buffer solution. Green, boosted shift by photoreceptor; Gray, linear shift with PBS buffer.

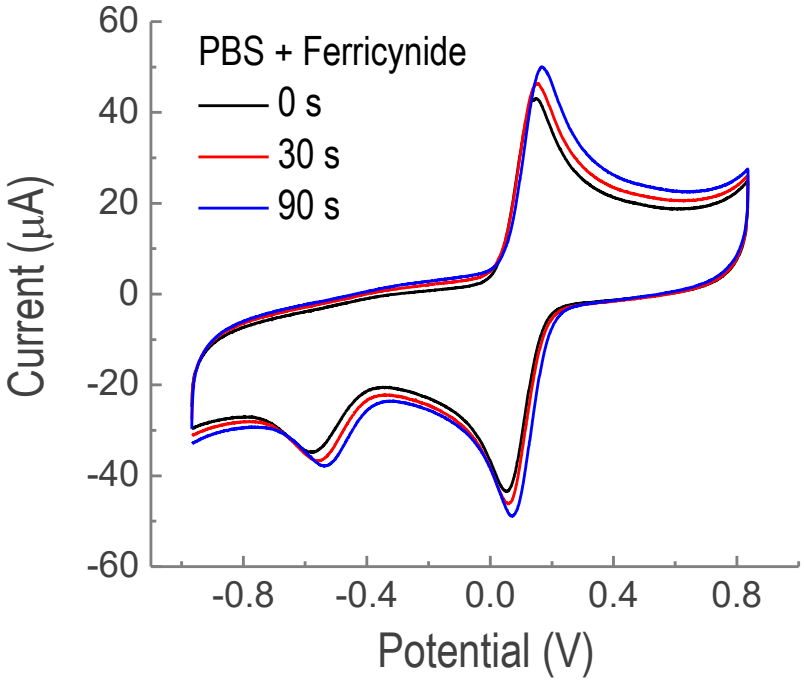

Figure S7. Linear shift of reduction peak potential in PBS and ferricynide blended solution for a duration of 30 s under white incident light. The oxygen reduction peak shifted from -0.6 V. Redox features of ferricynide were obtained over 0 V with peak shift.

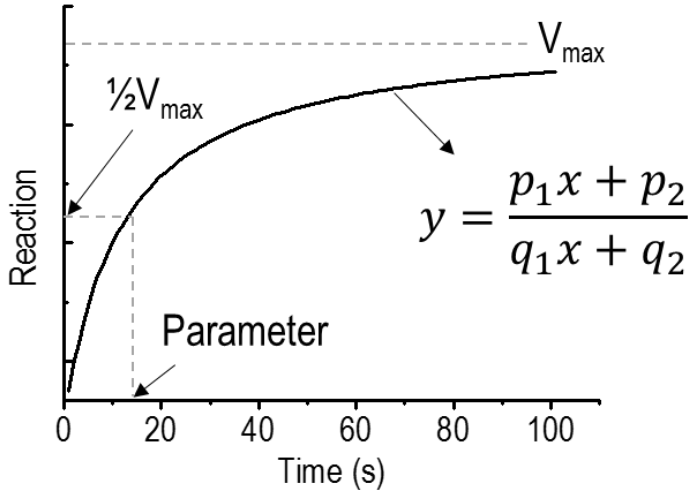

Figure S8. Voltammetry results according to exposing time by saturation behavior analysis with fitting equation (fractional expression).

For mathematical analysis, usual symbols (*x*, *y*, *dx*, *dy*, *dy/dx*, d^2y/dx^2) were used. In Fig. S8, each continuous incremental increase, *dx*, in *x* was less dominant at increasing *dy*. After saturation with very large value of *x*, the, maximum *y* was generated in the graph. As *x* was increased, fractional changes *dx/x* and *dy/y* were decreased. The positive slope (*dy/dx*) was steadily decreased. The second derivative (d^2y/dx^2) was also steadily decreased. It remained negative: $(d^2y/dx^2) = -|d^2y/dx^2|$.

From the general differential equation depending on specific integer of A and B, various natural phenomena could be described in the following:

$$\frac{(d^2y/dx^2)\cdot dx}{dy/dx} = A\cdot\left(\frac{dy}{y}\right) - B\cdot\left(\frac{dx}{x}\right) \qquad (1)$$

Each term is composed of fractional change. When A = B = 2, the second-order differential equation is obtained without empirical constants. This equation can describe the saturation behavior in our results with RPS as shown in Fig. S8. Setting *s* = slope = *dy*/*dx* gives the following:

$$\frac{ds}{s} = 2 \cdot \left(\frac{dy}{y} - \frac{dx}{x} \right) \quad (2)$$

where *ds/s* is the fractional change in the slope. Integrating and applying anti-logarithms leads the first-order differential equation for the slope, s:

$$s = \frac{dy}{dx} = C \cdot \left(\frac{y}{x} \right)^2 \quad (3)$$

$$y = \frac{p_1 x + p_2}{q_1 x + q_2} \quad (4)$$

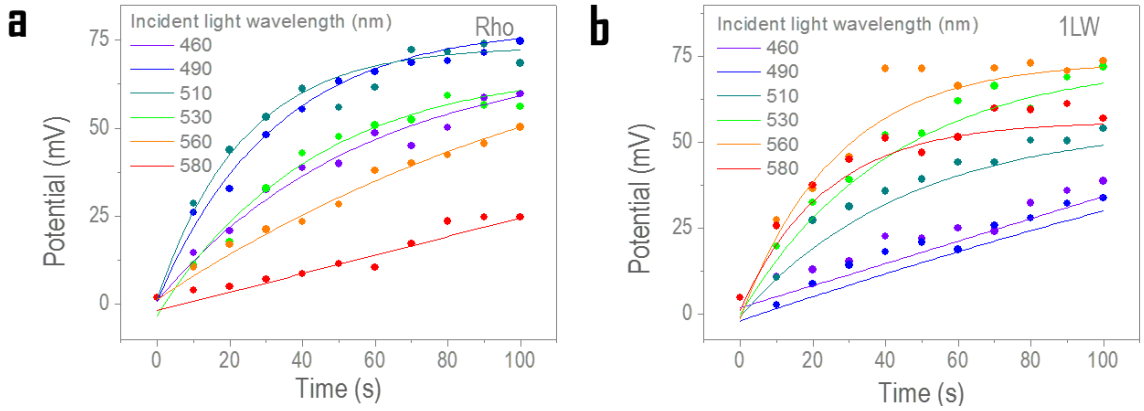

Figure S9. Curves of RPS in (a) Rho and (b) 1LW under different wavelength of incident light.